INELASTIC BEHAVIOR OF STEEL BEAM-COLUMNS OF BOX SECTION UNDER THE CONSTANT VERTICAL AND ALTERNATING HORIZONTAL LOADS

C. Matsui (I)
S. Morino (II)
K. Tsuda (III)
Presenting Author: K.Tsuda

SUMMARY

Steel beam-columns of box section are tested under the constant vertical and two-dimensional monotonic or cyclic horizontal loads. Experimental behavior is compared with the results of elasto-plastic and rigid-plastic analyses. It is shown that the post local buckling behavior of specimens with large values of width-thickness ratio B/t is well predicted by the rigid-plastic analysis considering the influence of local buckling, and that the conventional strength formula is too conservative.

INTRODUCTION

In conjunction with the seismic design, a number of investigations have been performed to make clear the cyclic behavior of structural members and frames subjected to the combined vertical and horizontal loads, in which the local and lateral buckling take place. However, the most of them are limited to the case of wide-flange members, and few researches have been reported on the inelastic behavior of steel beam-columns of box section. Particularly no research can be found on the three-dimensional inelastic behavior of the box members.

The paper presents the results of experimental and theoretical studies on the behavior of steel beam-columns of box section under the constant vertical and two-dimensional monotonic or alternating horizontal loads.

TEST PROGRAM

The test specimen is a cantilever column of a cold-formed box section as shown in Fig. 1, of which material is a mild steel (STKR41 or SS41, Japanese Industrial Standards). First, the constant vertical load P, and then the horizontal load H are applied to the specimen. Loading apparatus shown in Fig. 2 is designed to satisfy the condition that the following six components of the displacements at the top of the specimen must be kept free; the axial and two-directional sway displacements, the two-directional flexural rotations, and the torsional rotation [1]. As the experimental parameters, the width-thickness ratio B/t, the vertical load ratio $n = P/P_y$ and the direction of the horizontal load α are selected, and they vary as follows; $B/t = 22 - 47$, $n = 0.1, 0.3, 0.5$ and $\alpha = 0°, 15°, 30°, 45°$. The loading program employed for the horizontal load is as follows: Specimens in Series I are subjected to basically the monotonic

(I) Professor, Dept. of Architecture, Faculty of Engineering, Kyushu Univ., Hakozaki, Higashi-ku, Fukuoka-shi, 812 Japan.
(II) Professor, Dept. of Architecture, Faculty of Engineering, Mie Univ., Kamihama-cho, Tsu-shi, 514 Japan.
(III) Research Assistant, Dept. of Architecture, Faculty of Engineering, Kyushu Univ..

horizontal load, and one cycle of reversed loading is applied at the large amplitude of plastic deflection. Specimens in Series II are tested under the cyclic loading, where the amplitude of displacement $\bar{u}$ (see Fig. 1) is increased by 2/3 % of the column height ℓ in a stepwise manner every four cycles of loading completed. The specimen name is indicated in the form of A - BC D - EF, where A stands for series name, BC width-thickness ratio of column section B/t , D vertical load ratio (n = 0.1, 0.3 and 0.5, when D = 1, 3 and 5 respectively) and EF direction of the horizontal load α. Dimensions of the cross sections are shown in Table 1, together with the width-thickness ratio and the material. Forty eight specimens are tested.

THEORETICAL ANALYSIS

Two types of the theoretical analyses are performed to obtain the load-deflection curves of the cantilever beam-columns under the monotonic uniaxial bending; the rigid-plastic analysis considering the influence of local buckling, and the elasto-plastic analysis taking the spread of plastic zone into account.

Rigid-Plastic analysis Deterioration of the restoring force of the box steel beam-columns is mainly due to the local buckling, since the lateral buckling does not take place. Rigid-plastic analysis based on the technique used for the wide-flange member in Ref.[2] is performed to investigate the post local buckling behavior.

The deformed configuration of the cantilever column at the post local buckling state is idealized as shown in Fig. 3, and the problem is how to obtain $M-\Theta$ relations at the plastic hinge. By assuming the local buckling mechanism as shown in Fig. 4, the principle of virtual velocities can be written as follows[2]:

$$M = -P\,(\eta - 0.5)\,d + D_p / \dot{\Theta} \qquad (1)$$

where M denotes the applied moment at the plastic hinge, P the constant vertical load, ηd the distance between compressive flange and neutral axis, d the web depth, $\dot{\Theta}$ the virtual angular velocity of the plastic hinge, and D_p the rate of internal energy dissipation. The prime assumptions to estimate the value of D_p appearing in Eq. (1) are as follows: 1) Deformations are small. 2) Relative strains at the plastic hinge are proportional to the distance from the neutral axis. 3) Plate elements are in state of the plane stress. 4) The material has a rigid-perfectly-plastic characteristic conforming to the yield condition of von Mises.

The value of D_p is dependent on 4 variables ζ, ψ, η and δ_s (see Fig. 4) that define the form of the local buckling mechanism, and therefore the resisting moment M in Eq. (1) is also dependent on them. Based on the plastic upper bound theorem, the minimum resisting moment among the values computed by Eq. (1) gives a correct solution. In order to simplify the numerical analysis, it is tacitly assumed that the values of ζ and ψ which make the moment minimum when $\Theta/\Theta_{pc} = 5$ are valid for other values of Θ/Θ_{pc}, where Θ_{pc} denotes the elastic limit rotation. Moment-rotation relation is obtained by repeating the computation of the moment for a given value of δ_s.

Elasto-Plastic Analysis In addition to the rigid-plastic analysis, the elasto-plastic analysis is performed to investigate the behavior of beam-

columns in the absence of the local buckling. First, the moment-curvature relation is established from the Bernoulli-Euler hypothesis, based on the multi-linear stress-strain relation which idealizes results of the tensile coupon test. Deflection is then computed by integrating the curvature which is defined by the moment-curvature relation according to the moment distribution. The numerical computation is a nonlinear, iterative task.

RESULTS AND DISCUSSIONS

Behavior under Uniaxial Bending Examples of the load-deflection relations of Series I are shown in Figs. 5 and 6. In Fig. 5, the experimental results are shown by solid lines with circles, and the results of the elasto-plastic analysis and the rigid-plastic analysis are shown by dash-dot and dash-dot-dot lines, respectively. In specimens of B/t equal to 47, the result of the elasto-plastic analysis considering the influence of residual stress is shown by a broken line. Experimental curves are compared in Fig. 6. Definition of the symbols used is given in Fig. 7.

In Fig. 5, the points of flange and web local buckling observed initially are marked by ∇ and $\blacktriangledown$, respectively. It is observed from the test results that a considerable deterioration of the restoring force starts at the occurrence of the web local buckling induced after the flange buckling. Some specimens with large value of B/t can not attain the strength given by the mechanism curve, which is obtained from the second order plastic analysis by assuming a plastic hinge forming at the base of the beam-column. This phenomenon is more pronounced with the increase in the value of the vertical load ratio n. The deterioration of the restoring force becomes more apparent as the value of B/t becomes large, but an important difference is not observed in specimens with the value of B/t over 31. As to the theoretical results, the experimental behavior can be predicted to some degree by the elasto-plastic analysis up to the maximum load, while the rigid-plastic analysis considering the influence of local buckling can estimate the behavior of specimens with large value of B/t after the maximum load attained. Figure 8 shows the experimental results of cyclic behavior. The load carrying capacity decreases in each cycle of loading after the occurrence of local buckling. As to the influence of B/t and n, the tendency similar to the case of the monotonic behavior mentioned above is observed.

Figure 9 shows the relations between the nondimensional strain $\varepsilon_{cr}/\varepsilon_y$ at the occurrence of local buckling and $(B/t)\sqrt{\sigma_y/E}$, where σ_y denotes the yield stress, ε_y the yield strain, and E Young's modulus. Figure 10 shows the relations between the deformation capacity R defined in Fig. 11 and $(B/t)\sqrt{\sigma_y/E}$. With the increase in the value of $(B/t)\sqrt{\sigma_y/E}$, the strain ε_{cr} and the deformation capacity R become small. It seems in Figs. 9 and 10 that the deformation capacity is considerably small when the local buckling takes place within the range of $\varepsilon_{cr}/\varepsilon_y$ less than 2.

Behavior under Biaxial Bending Examples of the load-deflection relations of specimens subjected to biaxial bending are shown in Fig. 12, and the deflection paths are shown in Fig. 13. Definition of symbols appearing in figures is given in Figs. 1 and 14. In Fig. 14, the mechanism curve is obtained without regarding the influence of local buckling. As observed in the case of uniaxial bending, Fig. 12 shows the drastic deterioration of the restoring force in the range of large deflection, which is caused by the successive buckling of plate elements subjected to compression.

Strength Formula Figure 15 shows the experimental results of the maximum horizontal loads compared with the values computed by a strength formula given in Ref.[3],

$$\frac{N}{N_{cr}} + \frac{C_x M_x}{\left(1 - \frac{N}{N_{ex}}\right) M_{px}} + \frac{C_y M_y}{\left(1 - \frac{N}{N_{ey}}\right) M_{py}} = 1.0 \qquad (2)$$

in which N denotes the axial load, Ncr the critical load, N_e Euler buckling load, M the applied moment, M_p the full plastic moment, and C is the factor computed in relation to the moment gradient. Subscripts x and y indicate quantities computed about x- and y-axes, respectively. The value of Ncr is computed from the column curve formula in Ref.[3], taking the effective length equal to 2ℓ. Examples of m-n and m_x-m_y relations are shown in Figs. 16 and 17, respectively, in which the definition of symbols is given in Fig.18. In Figs. 16 and 17, the strength given by Eq. (2) (dash-dot line) and the full plastic strength (broken line) are shown together with the experimental results. The ratio of the experimental maximum load Hmax to the strength Hf computed by Eq.(2) ranges from 0.72 to 2.3. In the case of the uniaxial bending, the strength formula, Eq. (2) , gives fairly well, conservative estimate to the experimental maximum loads, except for the specimens of B/t equal to 47. It seemes in Fig. 15 that the strength formula is too conservative in the case of biaxial bending, and this conservative discrepancy becomes larger with the increase in the vertical load and the direction of the horizontal load α. The value of H_{max}/H_f is not much affected by the value of B/t. In Fig. 17, m_x-m_y curves obtained by connecting the experimental results resemble the interaction curve for the full plastic strength, and thus the linear interaction formula, Eq. (2) , which is extended from the formula for the uniaxial bending, cannot estimate the maximum loads of beam-columns subjected to the biaxial bending in a similar degree of accuracy for the uniaxial bending cases.

CONCLUSIONS

(1) In specimens subjected to uniaxial bending, a considerable deterioration of the restoring force starts at the occurrence of the web local buckling induced after the flange buckling, and the deterioration becomes drastic as the value of B/t increases.

(2) In specimens subjected to biaxial bending, the direction of sway does not coincide with the direction of the horizontal load α after the local buckling takes place, particularly when the vertical load is large.

(3) The conventional strength formula used in the plastic design of steel structures is too conservative in the case of biaxial bending.

(4) Experimental behavior of specimens with large value of B/t is well predicted by the rigid-plastic analysis considering the influence of local buckling.

REFERENCES

[1] Matsui, C., Morino, S. and Tsuda, K. : INELASTIC BEHAVIOR OF WIDE-FLANGE BEAM-COLMNS UNDER CONSTANT VERTICAL AND TWO-DIMENSIONAL ALTERNATING HORIZONTAL LOADS, Proc. of 7th WCEE, Istanbul, Sept. 1980, Vol.7, pp.39-46.

[2] Mitani, I. and Makino, M. : POST LOCAL BUCKLING BEHAVIOR AND PLASTIC ROTATION CAPACITY OF STEEL BEAM-COLUMNS, Proc. of 7th WCEE, Istanbul, Sept. 1980, Vol.6, pp.493-500.

[3] Architectural Institute of Japan : GUIDE TO THE PLASTIC DESIGN OF STEEL STRUCTURES, 1975, pp.129 (in Japanese).

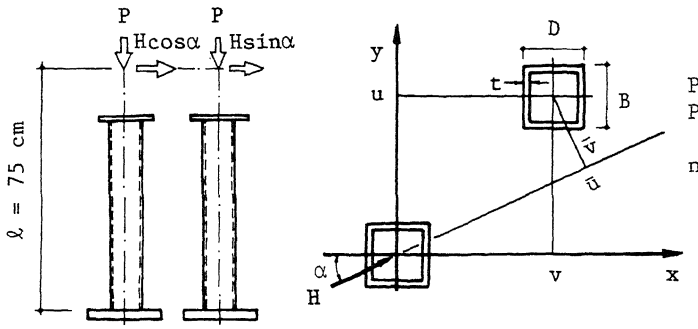

P ; axial load on a column
P_y; axial yield strength of a column
n ; vertical load ratio
$n=P/P_y$

Fig.1 Cantilever Column and Coordinates

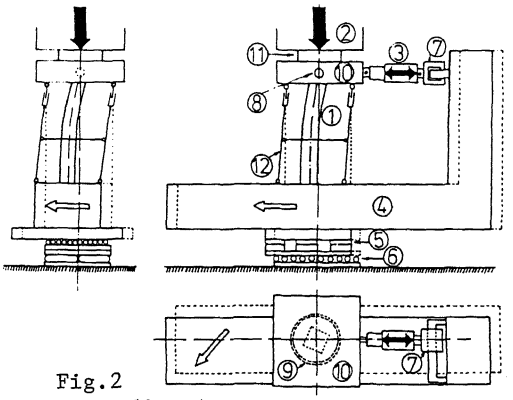

① Specimen
② Amsler Type Testing Machine
③ Hydraulic Jack
④ Loading Frame
⑤ ⑥ Two-Directional Rollers
⑦ Rollers
⑧ Two-Directional Hinge
⑨ Radial Bearing
⑩ Loading Plate
⑪ Thrust Bearing
⑫ Supporting Frame

Fig.2
Loading Apparatus

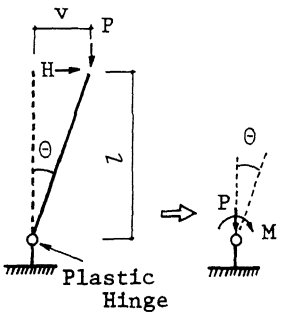

Fig.3
Model of Analysis

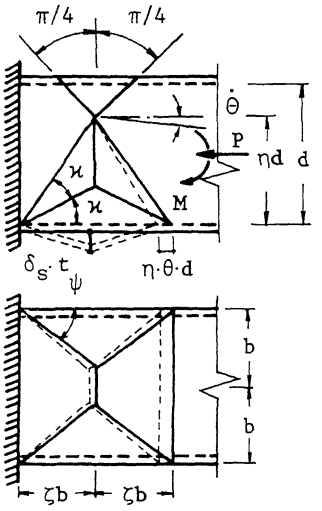

Fig.4
Local Buckling Mechanism

Table 1 Dimensions of the Cross Section

Column Section (mm) B x D x t	B/t	Material
□ - 150x150x3.2	47	SS41
□ - 150x150x4.5	33	STKR41
□ - 150x150x6.0	25	STKR41
□ - 100x100x3.2	31	STKR41
□ - 100x100x4.5	22	STKR41

B = width
D = depth
t = thickness

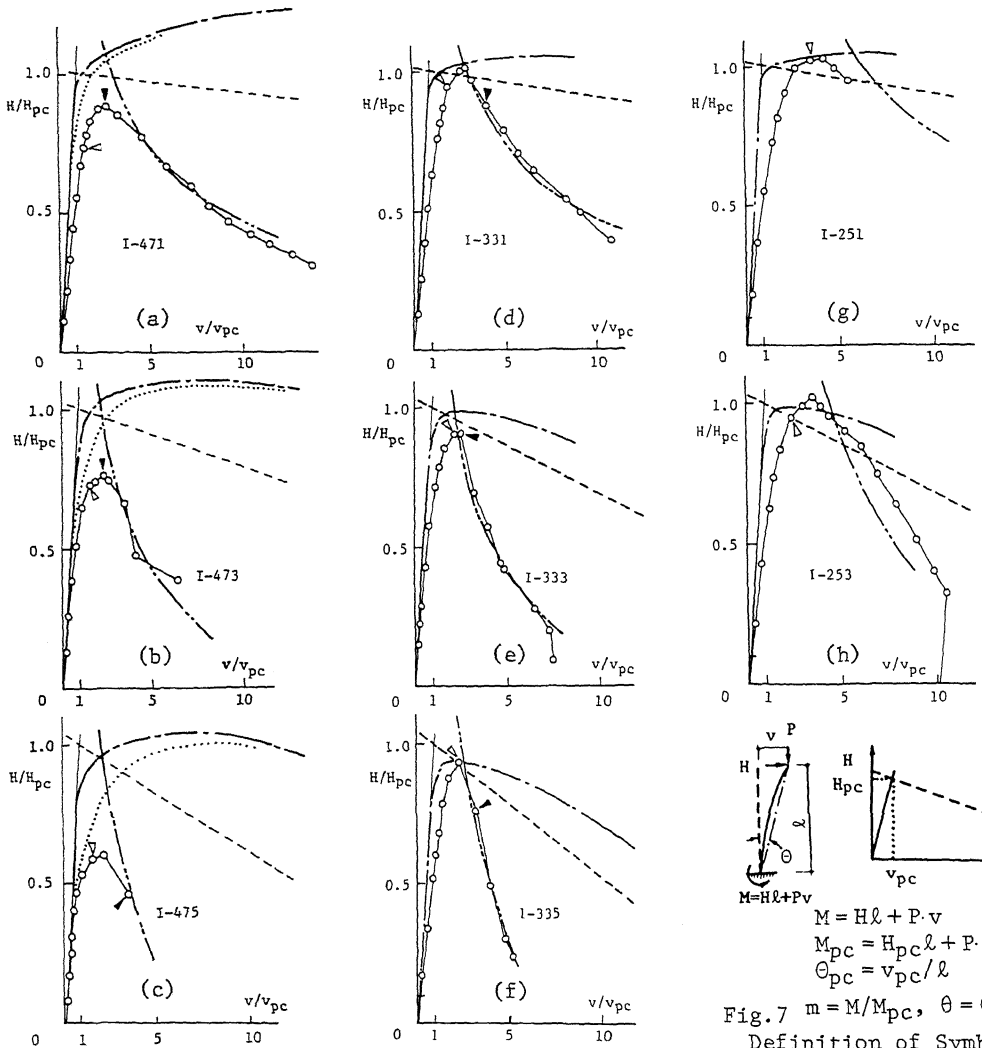

Fig.5 Load-Deflection Relations under Uniaxial Bending

$M = H\ell + P \cdot v$

$M_{pc} = H_{pc}\ell + P \cdot v_{pc}$

$\theta_{pc} = v_{pc}/\ell$

Fig.7 $m = M/M_{pc}$, $\theta = \theta/\theta_{pc}$ Definition of Symbols

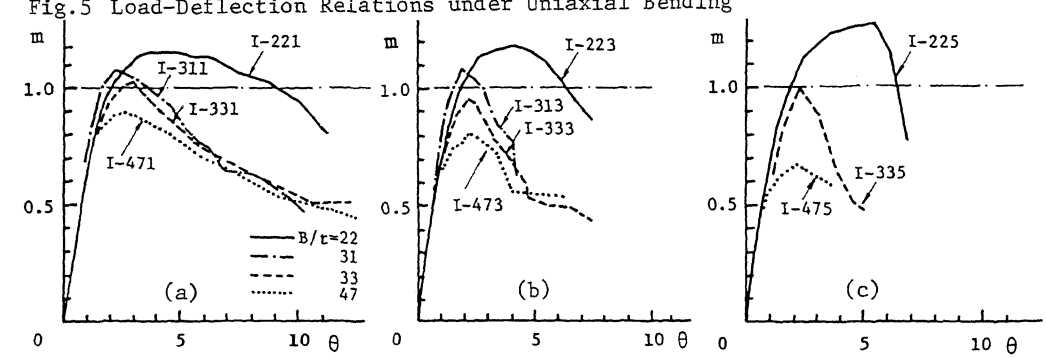

Fig.6 Moment-Rotation Relations

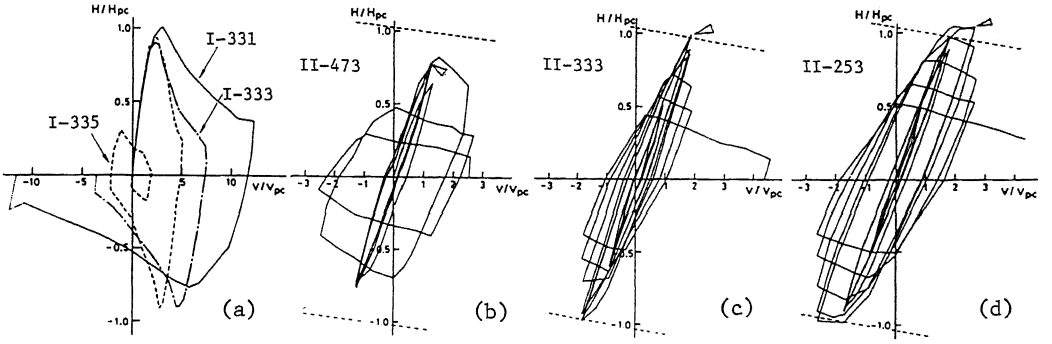

Fig.8 Cyclic Load-Deflection Relations

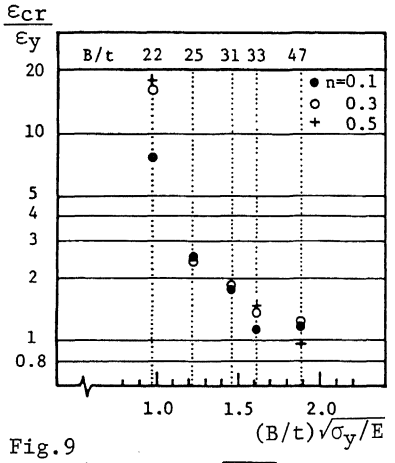

Fig.9
$\varepsilon_{cr}/\varepsilon_y - (B/t)\sqrt{\sigma_y/E}$ Relations

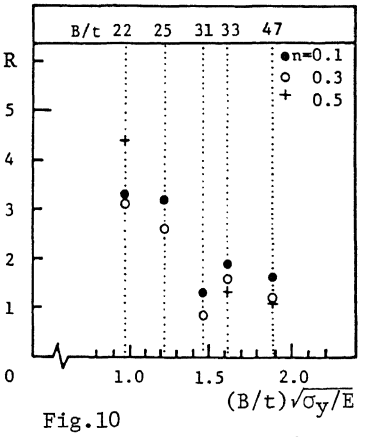

Fig.10
Deformation Capacity

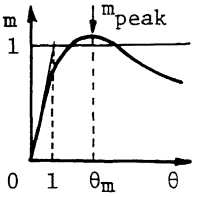

Fig.11
Definition of R

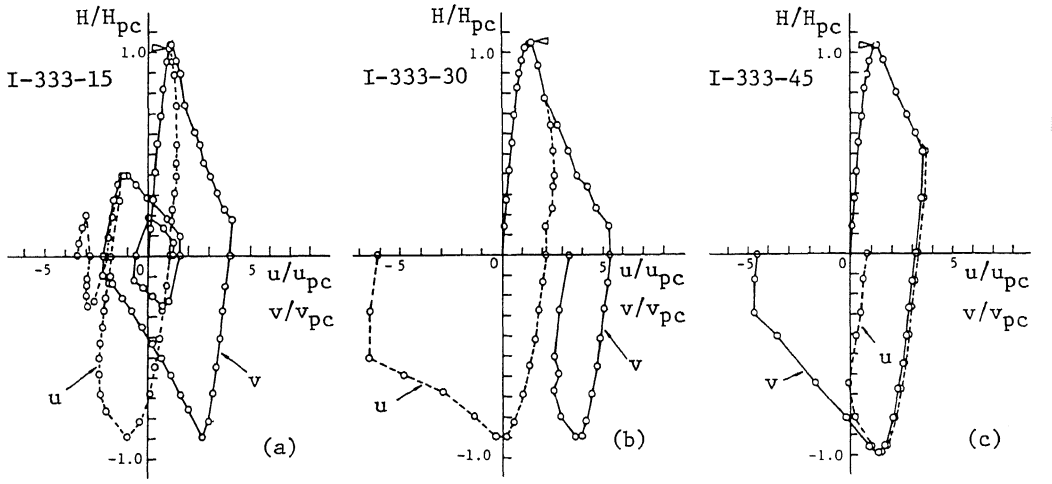

Fig.12 Load-Deflection Relations under Biaxial Bending

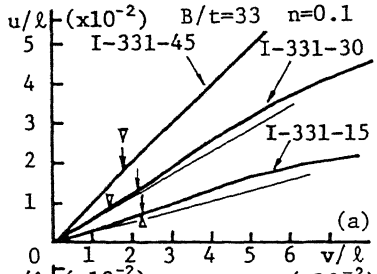

Fig.13 Deflection Path

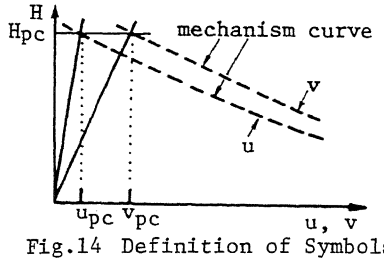

Fig.14 Definition of Symbols

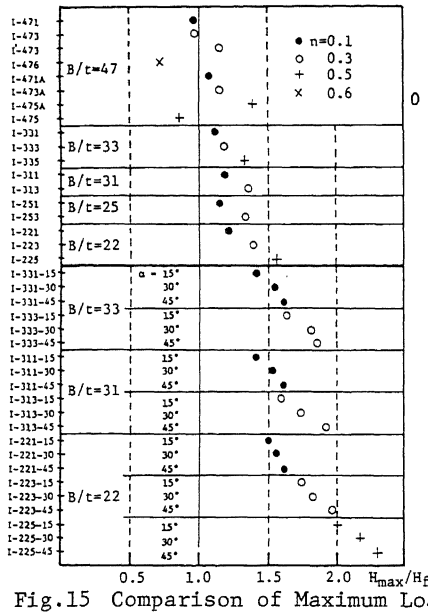

Fig.15 Comparison of Maximum Load

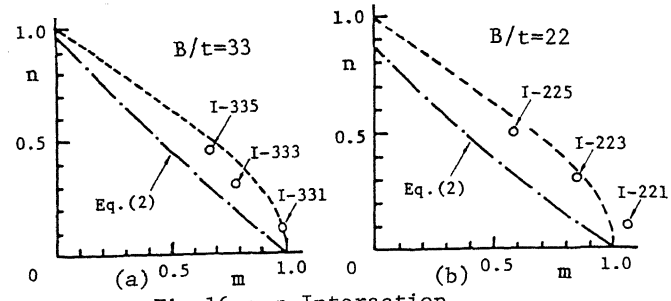

Fig.16 m-n Interaction

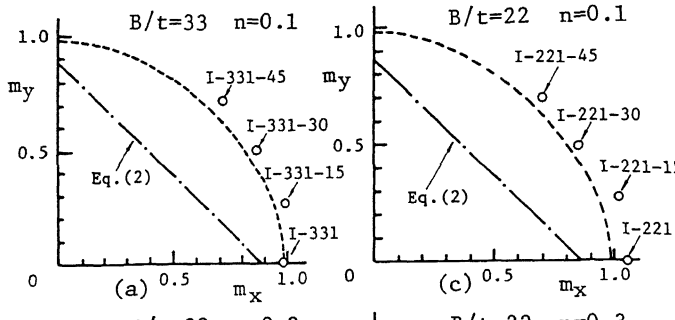

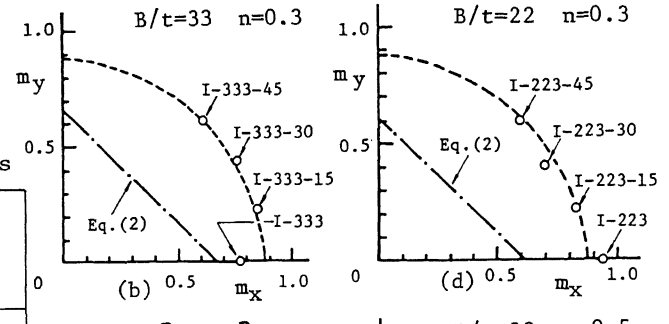

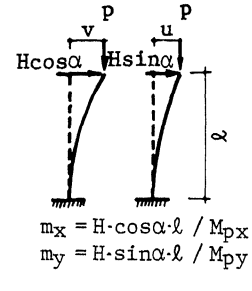

Fig.18 Definition of Symbols

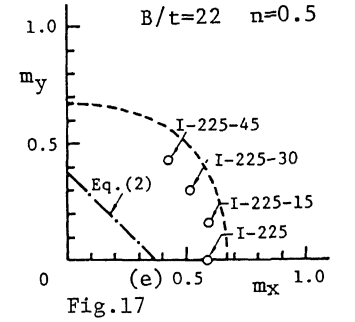

Fig.17 m_x-m_y Interaction